Water Resources Research

RESEARCH ARTICLE
10.1029/2019WR026966

Bayesian Calibration and Validation of a Large-Scale and Time-Demanding Sediment Transport Model

Felix Beckers[1], Andrés Heredia[1,2,3], Markus Noack[1,4], Wolfgang Nowak[2], Silke Wieprecht[1], and Sergey Oladyshkin[2]

[1]Institute for Modelling Hydraulic and Environmental Systems, Department of Hydraulic Engineering and Water Resources Management, University of Stuttgart, Stuttgart, Germany, [2]Institute for Modelling Hydraulic and Environmental Systems, Department of Stochastic Simulation and Safety Research for Hydrosystems, SC SimTech, University of Stuttgart, Stuttgart, Germany, [3]Faculty of Civil Engineering, Universidad Politécnica Salesiana, Quito, Ecuador, [4]Faculty of Architecture and Civil Engineering, Karlsruhe University of Applied Science, Karlsruhe, Germany

Abstract This study suggests a stochastic Bayesian approach for calibrating and validating morphodynamic sediment transport models and for quantifying parametric uncertainties in order to alleviate limitations of conventional (manual, deterministic) calibration procedures. The applicability of our method is shown for a large-scale (11.0 km) and time-demanding (9.14 hr for the period 2002–2013) 2-D morphodynamic sediment transport model of the Lower River Salzach and for three most sensitive input parameters (critical Shields parameter, grain roughness, and grain size distribution). Since Bayesian methods require a significant number of simulation runs, this work proposes to construct a surrogate model, here with the arbitrary polynomial chaos technique. The surrogate model is constructed from a limited set of runs ($n = 20$) of the full complex sediment transport model. Then, Monte Carlo-based techniques for Bayesian calibration are used with the surrogate model (10^5 realizations in 4 hr). The results demonstrate that following Bayesian principles and iterative Bayesian updating of the surrogate model (10 iterations) enables to identify the most probable ranges of the three calibration parameters. Model verification based on the maximum a posteriori parameter combination indicates that the surrogate model accurately replicates the morphodynamic behavior of the sediment transport model for both calibration (RMSE = 0.31 m) and validation (RMSE = 0.42 m). Furthermore, it is shown that the surrogate model is highly effective in lowering the total computational time for Bayesian calibration, validation, and uncertainty analysis. As a whole, this provides more realistic calibration and validation of morphodynamic sediment transport models with quantified uncertainty in less time compared to conventional calibration procedures.

Key Points:
- We reduce a time-demanding sediment transport model with a surrogate technique based on the arbitrary polynomial chaos expansion (aPC)
- Bayesian model calibration and validation in a fraction of computational time compared to conventional (manual, deterministic) methods
- We achieve a more realistic calibration, a more successful validation, and valuable information in the form of uncertainty intervals

Supporting Information:
- Supporting Information S1

Correspondence to:
F. Beckers,
felix.beckers@iws.uni-stuttgart.de

Citation:
Beckers, F., Heredia, A., Noack, M., Nowak, W., Wieprecht, S., & Oladyshkin, S. (2020). Bayesian calibration and validation of a large-scale and time-demanding sediment transport model. *Water Resources Research*, *56*, e2019WR026966. https://doi.org/10.1029/2019WR026966

Received 15 DEC 2019
Accepted 12 JUN 2020
Accepted article online 15 JUN 2020

1. Introduction

Rivers have political, economic, and environmental relevance and have been of great importance for the development of urban regions (Kostof & Castillo, 2005). Many rivers have undergone anthropogenic change during this development (Kondolf & Pinto, 2017). Such change includes the reduction of flood plain areas due to settlement, river course simplification achieved by straightening and narrowing, and the construction of hydraulic structures for a variety of purposes (e.g., for bank/bed protection, improved navigability, hydropower production). As a result of these measures, the natural hydromorphodynamic behavior of river systems has been changed, and excessive erosion and deposition can be a medium to long-term consequence (e.g., Habersack & Pigay, 2007; Hinderer et al., 2013; Reisenbüchler et al., 2019; Stecca et al., 2019). To study these consequences, physical-deterministic numerical models are in use. They are capable to reproduce the hydromorphodynamic system behavior to predict sediment transport processes and riverbed evolution (James et al., 2010; Pinto et al., 2012).

By now, many morphodynamic sediment transport models exist and numerical methods are constantly improving. Despite this, challenges remain since accurate computational description of sediment dynamics requires to include several model- and river-specific parameters, which results in highly parameterized models (e.g., Merritt et al., 2003). Many of the model-specific parameters are based on empirical approaches (e.g., critical Shields parameter), and most of the river-specific parameters are extremely difficult to measure in both space and time (e.g., grain size distribution in the surface and subsurface layer, sediment transport rates, or transported grain sizes). Additionally, monitoring programs are rarely continuously available for

long-term periods (Hinderer et al., 2013), which explains why information on river-specific parameters is often confined to local surveys. These model- and river-specific parameters carry a large degree of uncertainty that must be thoroughly considered during modeling (e.g., Schmelter et al., 2012; Villaret et al., 2016). Consequently, sediment transport models require a reasonable calibration and validation process to evaluate the reliability, accuracy, and quality of the model results (Merritt et al., 2003; Simons et al., 2000). Model calibration is performed by adjusting independent and uncertain model- and river-specific parameters within a physically meaningful range to reproduce as faithfully as possible the morphodynamic changes observed in the field within a given period (Cunge et al., 1980; Maren & Wegen, 2016; Oreskes et al., 1994; Simons et al., 2000). In the following validation process, the model response is tested on an independent morphodynamic data set with the selected parameters found during calibration.

The conventional approach in morphodynamic model calibration is manual calibration through heuristic exercise: The calibration parameters are manually adjusted and the simulation results are checked after each model run. This iterative procedure results in a single, allegedly best solution. Unfortunately, the combination of required model runs and constant monitoring of results leads to a labor-intensive and time-consuming workflow, especially for large-scale and time-demanding morphodynamic models (e.g., Klar et al., 2012, 2014; Mohammadi et al., 2018). Another challenge is related to the possible ill-posedness of the calibration problem, that is, the model can achieve similar calibration quality under different parameter combinations representing different river conditions (Chavarrías et al., 2018). This, in turn, means that a unique deterministic solution does not exist and additionally increases the complexity of calibration. Thus, manual calibration techniques may be criticized because of the total time requirement and potential for subjective bias on the part of the modeler when selecting one deterministic solution among multiple potential solutions (e.g., Muehleisen & Bergerson, 2016; Schmelter et al., 2012).

One possibility for handling these challenges would be accounting for the uncertainty in the calibration parameters and their resulting values by applying a stochastic calibration. Contrary to the deterministic approach (one best solution), a stochastic calibration approach conceptualizes the values of calibration parameters and model results as random variables (e.g., Kim & Park, 2016). Random variables mean that a range of values are admitted, where each possible value is equipped with an associated probability or probability density. Thus, multiple possible solutions, occurring in proportion to how likely they are, will match data and assumptions. During stochastic calibration, the main goal is not only to match the measurements as closely as possible with the simulation results, but additionally to assess the precalibration through postcalibration uncertainty and to reduce, in a manner consistent with the measurements, the uncertainty through modification of the model inputs (Muehleisen & Bergerson, 2016). A well-known stochastic calibration approach is Bayesian inference, where the goal is to learn about the unknowns (i.e., calibration parameters) given observed or measured data (Box & Tiao, 1973). The approach allows for the inclusion of a prior idea or information about the unknowns via prior probability distributions and also information about how observed data depend on the unknowns through a likelihood function. Thus, the Bayesian framework infers a posterior distribution (multiple solutions) of the unknowns in light of known information. This procedure ensures that linear and nonlinear model relations are accounted for and that corresponding uncertainties are quantified, both of which can hardly be realized through a manual approach.

Although widely employed in a variety of related disciplines such as ecology, hydrology, and environmental sciences (see Schmelter et al., 2011), little information on Bayesian approaches in sediment transport modeling are available as they are relatively new in fluvial sediment transport (Schmelter & Stevens, 2013). Wu and Chen (2009) attribute this to the little resemblance of Bayesian methods to conventional (deterministic) approaches for parameter estimations and missing demonstration to hydraulic engineers. These authors employ a Bayesian framework to update parameters of a sediment entrainment model and obtain more accurate and realistic results after Bayesian updating (Wu & Chen, 2009). Schmelter et al. (2011) introduce a Bayesian sediment transport model for unisize bed load and employ it to a pedagogical sediment transport problem. Schmelter et al. (2012) extend this model and demonstrate the applicability to a large gravel river for sediment budget predictions. In the study of Schmelter and Stevens (2013), the authors present potential benefits of a Bayesian statistical approach over a traditional curve-fitting approach to simulate critical stresses observed in laboratory flume experiments. More recent studies are available from Mohammadi et al. (2018), who present a benchmark study on Bayesian selection of hydromorphodynamic models under computational time constraints and Shojaeezadeh et al. (2018) who use a Bayesian network to model

stochastically the suspended sediment load given river discharge volumes. Independently of each other, all these studies recommend the use of Bayesian methods in the field of sediment transport modeling due to their various benefits including uncertainty quantification, parameter estimation, or model selection to finally obtain more robust and confident predictions. For this reason, Schmelter et al. (2011) generally conclude that Bayesian modeling can provide a tool for innovation in sediment transport research, though blind use of Bayesian principles could be misleading and requires quality control (Mohammadi et al., 2018). As it turns out, a stochastic calibration of a morphodynamic sediment transport model seems promising. However, the main drawback of Bayesian inference is that numerous calibration runs are necessary to obtain posterior distributions of the investigated parameters. Relatedly, a large number of model executions (i.e., independent realizations) would be necessary, which is unfeasible for a full complex large-scale and time-demanding sediment transport model. Hence, the limiting factor of Bayesian calibration in morphodynamic sediment transport modeling is the total time requirement, making model reduction techniques and surrogate models attractive.

The main goal of a surrogate model (also known as response surface, emulator, metamodel, reduced model, etc.) is to replicate the behavior of the full complex physical-deterministic model from a limited set of runs without sacrificing a lot of detail and accuracy. Therefore, intelligent input parameter combinations that cover the range of the parametric space as good as possible are strategically selected (called collocation points or training sets). Since surrogate models are an approximation of any full physical-deterministic model, they substantially reduce the computational effort, making them attractive to quantify the uncertainty in the real system using Bayesian statistics. Recent developments based on the polynomial chaos expansion technique (Wiener, 1938) express the stochastic solution of the surrogate model as orthogonal polynomials of the input parameters to achieve better convergence (e.g., Oladyshkin & Nowak, 2012). With this technique, a surrogate model can be constructed that is suitable even for very computationally demanding problems (Köppel et al., 2019). For example, it can treat morphodynamic sediment transport modeling including a profound uncertainty analysis followed by Bayesian model calibration.

This work proposes a Bayesian calibration of a large-scale and time-demanding morphodynamic sediment transport model of the Lower Salzach River (Germany, Austria) (Beckers et al., 2016). In an initial step, we will construct a surrogate model using the arbitrary polynomial chaos technique (aPC) (Oladyshkin & Nowak, 2012) based on sensitive calibration parameters in order to enable a stochastic analysis. The calibration will be achieved by implementing an iterative Bayesian update of the aPC surrogate model via a likelihood-controlled strategy (Oladyshkin, Schröder, et al., 2013), to match a necessary number of random Monte Carlo surrogate model realizations to available measurements of the riverbed. This Bayesian analysis identifies regions in the prior ranges of analyzed calibration parameters where the surrogate model achieves the best agreement with the measured data. Based on these findings, we aim to obtain an adequate posterior distribution of the calibration parameters, resulting in multiple suitable parameter combinations. In a next step, the calibration results will be validated against an additional set of measured riverbed data and we will provide the statistical information for both calibration and validation, in order to assess the quality of the stochastic analysis. Further, we will verify the approximations made during stochastic model inversion and the construction of the aPC surrogate model against the morphodynamic sediment transport model using the best deterministic solution from the posterior distribution. Finally, we will present the residuals of the riverbed evolution obtained with the stochastically calibrated surrogate and full complex model. Moreover, we will compare these findings with a manually calibrated morphodynamic sediment transport model (Beckers et al., 2016). We expect that obtaining statistical information will help to improve the reproduction of the morphodynamic processes, increase the robustness of the physical-deterministic sediment transport model and eventually result in a more reliable and realistic calibration in less time.

2. Materials and Methods

2.1. The Lower River Salzach

The River Salzach is an alpine river that originates in the Kitzbuehel Alps and drains via the River Inn to the River Danube. Many parts of the River Salzach have been subject to anthropogenic modifications that have changed the entire hydraulic and morphodynamic system behavior. Thus, restoration measures are discussed in order to restore a sustainable morphodynamic equilibrium (Habersack & Piégay, 2007).

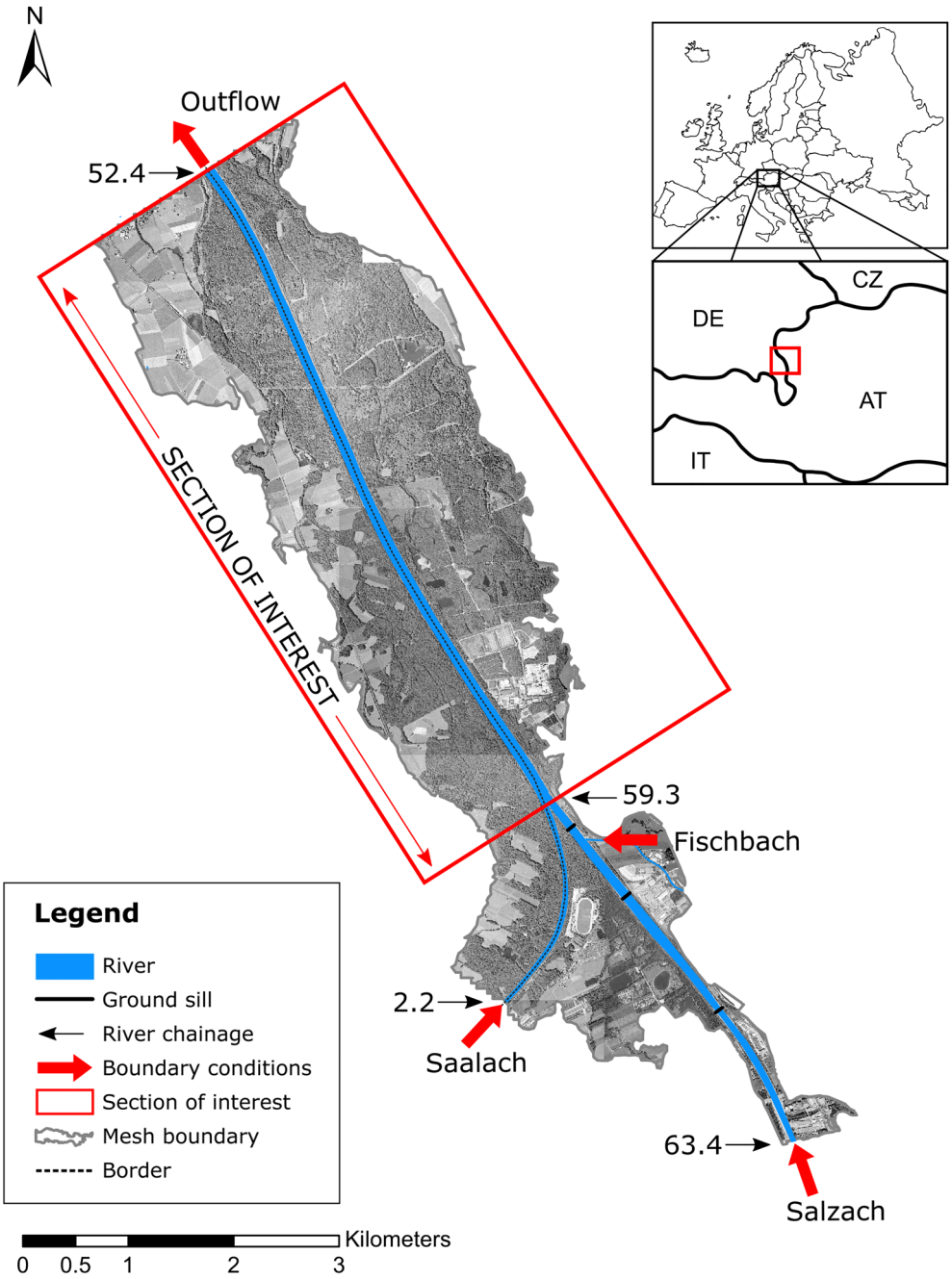

Figure 1. Overview of the study area in the Lower River Salzach (chainage 63.4 to 52.4 km). Riverbed erosion in the upstream section (chainage 63.4 to 59.3 km) is prevented due to three lateral structures (ground sills). The investigated section of interest covers the region downstream of the confluence with the River Saalach from river chainage 59.3 to 52.4 km.

Especially the German/Austrian section of the Lower River Salzach in the basin of Freilassing (47°51′32.1″N 12°59′50.2″E) has suffered from heavy river course modifications in the past. River course straightening, bank stabilization, and hindered longitudinal sediment continuity due to lateral engineering structures has led to restricted river dynamics, missing sediment supply, and an increased transport capacity. As a result, the presence of historically existing alternating gravel bars has declined. Further, the increased flow velocities and shear stresses have induced progressive riverbed erosion and have pushed the river into a critical erosion state. The constant risk of riverbed erosion was particularly evident during flood

events in August 2002 and June 2013. The peak discharge at the gaging station Laufen (chainage 47.0 km) during both flood events reached and exceeded the discharge of a 100-year flood ($Q_{100} = 3{,}100\ m^3s^{-1}$, $Q_{2002} = 3{,}000\ m^3s^{-1}$, $Q_{2013} = 3{,}530\ m^3s^{-1}$, for reference $Q_{mean}\ 240\ m^3s^{-1}$). Significant riverbed deepening was the consequence. The current situation of the Lower River Salzach is aggravated by the fact that only a thin layer of protective gravel material covers a layer of fine-grained and erosion-sensitive material due to altered sediment supply (Mangelsdorf et al., 2000). Once the protective material is eroded, rapid bed incision and deep scour formations are likely and have been already observed in upstream regions (Stephan et al., 2003). Moreover, the morphodynamic behavior of the Lower River Salzach is dominated by the sediment supply from the River Saalach that is the largest tributary. Thus, the hydromorphological situation of the Lower River Salzach requires measures that can mitigate the ongoing erosion process and protect the river from further morphological and environmental degradation without decreasing the degree of flood protection. To obtain an improved understanding of the morphodynamic system and to evaluate the long-term riverbed behavior, a 2-D morphodynamic sediment transport model of the Lower River Salzach using *Hydro_FT−2D* was applied by Beckers et al. (2016) on behalf of the water authorities of Traunstein (WWA) and of Salzburg (ASL).

2.2. The Morphodynamic Sediment Transport Modeling Software *Hydro_FT−2D*

The morphodynamic sediment transport modeling software *Hydro_FT−2D* (Nujic et al., 2019) is coupled with the hydraulic solver of the two-dimensional flow modeling software *Hydro_AS−2D* (Nujic & Hydrotec, 2017). Preprocessing and postprocessing of the 2-D mesh including mesh generation, definition of boundary conditions, and evaluation of simulation results is conducted with the software SMS (Surface-water Modeling System) (Aquaveo, 2013). *Hydro_FT−2D* solves the shallow water equations by means of a finite volume approach for spatial discretization and the explicit Runge-Kutta method for temporal discretization (Nujic & Hydrotec, 2017). Bed roughness coefficients are taken into account by Strickler values k_{St}, which are the reciprocals of Manning's values n ($k_{St} = 1/n$). Total roughness (k_{St}) and grain roughness $\left(k'_{St}\right)$ can be specified separately. Bed load can be calculated with the equation of Hunziker (1995), an extended form of the equation by Meyer-Peter and Mueller (1948), to consider multifraction transport (see also Hunziker & Jaeggi, 2002). Total load can be calculated with the equations of Engelund and Hansen (1967) or Ackers and White (1973). Sediment continuity to calculate riverbed evolution is ensured by solving the Exner (1925) equation. The software uses a multiple layer approach to simulate riverbed evolution and allows the use of multiple particle sizes d_i ($i = 1,...,n$ where $n_{max} = 12$) to reconstruct the stratification of the riverbed. The composition of the grain size distribution in the mixing layer is calculated using the approach of Hirano (1971), and the vertical exchange over the layers is calculated according to Hunziker (1995).

2.3. Model Setup of the Lower River Salzach and Data Availability

In comparison to the earlier model employed by Beckers et al. (2016), the model of the Lower River Salzach used in this study is slightly reduced in length (11.0 km instead of 13.2 km) because the main focus is set on the most relevant river section. This section is located downstream of the confluence with the River Saalach between river chainage 59.3 and 52.4 km. Consequently, the presented results are limited to this section of interest with a length of 6.9 km. Figure 1 gives an overview of the study area, the model domain, and the section of interest.

The applied model setup uses eight grain size classes (0.5, 2.0, 8.0, 16.0, 31.5, 63.0, 90.0, and 140.0 mm) to calculate bed load transport using the equation of Meyer-Peter and Mueller (1948) in the extended form by Hunziker (1995) (see also Hunziker & Jaeggi, 2002). Suspended load is not considered since the model aims at simulating the long-term riverbed behavior of the Lower River Salzach. The computational mesh consists of 16,113 elements (14,040 nodes) of which 1,525 elements (1,756 nodes) represent the movable riverbed in the entire Salzach and 950 elements (1,138 nodes) represent the movable riverbed in the section of interest (riverbanks are nonerodible, average movable width is approximately 82 m). The average cell size along the riverbed is 16 m in width and 36 m in length. The initial riverbed geometry is based on cross-section measurements of the year 2002, which are available at a regular distance of 200 m for the entire model domain. The typical slope is 0.11% for the upstream model region and reduces to 0.09% in the section of interest. In addition, cross-section measurements at the same distance are available for the years 2005, 2010, and

2013. Information on the grain size distribution is based on measurements that were conducted in different years (1991, 1993, 1996, and 2001) at only a few places in the river (total number of available measurements: eight for the surface layer and nine for the sublayer) and from previous studies (Beckers et al., 2016). The mean grain size diameter of the active layer and the sublayer is $d_{m,al} = 49.6$ mm and $d_{m,sl} = 45.8$ mm, respectively (values averaged over length and width). Three ground sills are located at a river chainage of 62.0, 60.6, and 59.8 km to prevent ongoing riverbed erosion in the upstream River Salzach. At these locations, the riverbed in the model is defined as nonerodible. Gaging stations at the rivers Salzach and Saalach provide the hydraulic input data. Bed load input from the upstream river regions (Salzach and Saalach) is considered using river-specific rating curves that are derived from measurements at a hydroelectric power plant located at Saalach chainage 2.4 km and available from previous studies (Beckers et al., 2016; Stephan et al., 2002). A small tributary (Fischbach) flows into the River Salzach at a chainage of 59.9 km. It is only considered hydraulically since bed load input from this tributary is negligible (Mangelsdorf et al., 2000; Stephan et al., 2002). The downstream boundary condition is defined as a constant energy slope of 0.1%. Further model parameterization includes a sediment density of 2,650 kg m^{-3}, a sediment porosity of 37%, and an active layer thickness that corresponds to the maximum grain size class d_{max}.

2.4. Previous Manual Calibration, Validation, and Uncertainty Analysis

Beckers et al. (2016) first calibrated and validated their model hydraulically against water level measurements to identify local changes in the total roughness composition along the main channel (13 regions identified, of them 8 in the section of interest). Subsequently, Beckers et al. (2016) manually calibrated their morphodynamic model for the period of 2002–2010 against the observed riverbed evolution (erosion and deposition) and validated the model for the period of 2010–2013. For these periods, Table 1 provides the minimum, mean, and maximum value of the hydraulic and morphological boundary conditions for the three upstream inflows Salzach, Saalach, and Fischbach. The hydrographs were reduced by a bed load relevant discharge threshold, which was found to be 350 $m^3 s^{-1}$ with regard to the total flow rate in the system (Sadid et al., 2016). It is worth noting, that the Saalach did not exceed a sediment input rate of 2,500 kg s^{-1} during these periods.

The manually calibrated and validated parameters were found by testing more than 200 parameter combinations (Beckers et al., 2016) in the same number of model runs. In this study, the accepted manually calibrated parameter combination is applied to the shortened model of the Lower River Salzach (Figure 1) for the equivalent periods (Table 1). The manually determined values of the calibration parameters are listed in Table 2. The table also summarizes the grain size classes as well as the total bed roughness coefficients found during their initial hydraulic calibration. For better comparison with the stochastically calibrated results, the roughness parameters are presented as weighted average over the existing mesh elements for the entire Salzach and for the section of interest.

The computation time for one run of the shortened model is about 7.14 hr for the calibration period (years 2002–2010) and 2.0 hr for the validation period (years 2010–2013) on a conventional computer with a maximum speed of 3.2 GHz (four cores). The model fit between simulation results and measured values results in a root-mean-square error of 0.68 m for the calibration period (2002–2010), and a root-mean-square error of 0.91 m for the validation period (2010–2013). Details are provided in section 3.5.

Beckers et al. (2018) applied the first-order second-moment method to quantify the uncertainties of the initial sediment transport model of the Lower River Salzach. The impact on model results have been evaluated for eight parameters including four model-specific parameters (critical Shields parameter, scaling factor of bed load transport equation, active layer thickness, acceleration factor) and four river-specific parameters (total roughness of river channel, grain roughness, bed load input of River Salzach and Saalach). The results indicate that the most sensitive parameters are the critical Shields parameter θ_{crit} and the grain roughness $k'_{St,j}$ among the model-specific and river-specific parameters, respectively.

2.5. Selection of Parameters for the Bayesian Calibration and Validation

In the current study we apply a Bayesian approach to stochastically calibrate and validate the morphodynamic model of the Lower River Salzach according to the measured riverbed geometry from the years 2002, 2005, 2010, and 2013. The selection of calibration parameters is based on the previous studies of Beckers et al. (2016, 2018). Included are the critical Shields parameter θ_{crit} (global parameter) and the

Table 1
Minimum (Q_{min}, $Q_{S,min}$), Mean (Q_{mean}, $Q_{S,mean}$), and Maximum Values (Q_{max}, $Q_{S,max}$) of Discharges (Q) and Sediment Input Rates (Q_S) for the Calibration (2002–2010) and Validation Period (2010–2013)

Period	Inflow	Q_{min} [$m^3\ s^{-1}$]	Q_{mean} [$m^3\ s^{-1}$]	Q_{max} [$m^3\ s^{-1}$]	$Q_{S,min}$ [$kg\ s^{-1}$]	$Q_{S,mean}$ [$kg\ s^{-1}$]	$Q_{S,max}$ [$kg\ s^{-1}$]
Calibration	Salzach	162	362	1,569	0	3	73
(2002-2010)	Saalach	24	91	810	0	13	2,500
	Fischbach	1	8	72	—	—	—
Validation	Salzach	171	380	2,281	0	6	259
(2010–2013)	Saalach	35	94	1,072	0	19	2,500
	Fischbach	1	8	99	—	—	—

grain roughness (k'_{St}) (local parameter). In the model of the Lower River Salzach, 13 different regions of total roughness exist that stem from the hydraulic calibration (Table 2). This is why the varied grain roughness is denoted as $k'_{St,j}$ $(j = 1,...,13)$. In addition, the grain size distribution d_i $(i = 1,...,8)$ is selected as third calibration parameter to account for the uncertainty in the grain sizes given their year of sampling (1991, 1993, 1996, and 2001), their low number of available measurements (surface layer: eight samples, sublayer: nine samples), and the potentially underestimated surface armoring. Since the grain size distribution takes into consideration the uncertainty in the measured data but is also used as a pure numeric calibration parameter in some sediment transport models, it can be considered both a model- and river-specific parameter.

In order to define the allowable range of variation in the selected calibration parameters as prior probability distributions, an additional preliminary sensitivity analysis based on 16 model runs was conducted. This was done to account for any changes regarding sensitivity in the shortened model and to test the additional parameter grain size distribution. The range of variation for the Bayesian calibration is generated by deviating each selected parameter θ_{crit}, $k'_{St,j}$, and d_i between a minimum and maximum value considering the physical meaning of each parameter and the results of the preliminary sensitivity analysis. Thus, the prior assumption for each of the three calibration parameters can be represented in their limits via uniform distributions as $\omega_{\theta_{crit}} \sim U(0.033,\ 0.047)$, $\omega_{k'_{St}} \sim U(-4,\ +4)$ and $\omega_d \sim U(-0.2, +4)$, and the uncertain parameters form the following vector $\omega = \{\omega_{\theta_{crit}}, \omega_{k'_{St}}, \omega_d\}$. Uniform distributions are used to avoid any subjective elicitation on the distribution shape of the parameters. It is worth noting that $k'_{St,j}$ is varied relatively to the initial grain roughness values (Table 2). Likewise, we relatively vary the globally defined grain size classes d_i and not the volumetric composition (Table 2). Consequently, the related physical parameters are $\omega_{\theta_{crit}}$, $k'_{St,j} + \omega_{k'_{St}}$

Table 2
Total Roughness, Grain Size Classes and Manually Determined Calibration Values of Grain Roughness and Critical Shields Parameter

Model parameters		Values applied	Comment or additional information
Total roughness	$k'_{St,j}[m^{1/3}s{-}^{1}]$	29.6*/28.3**	Weighted average over mesh elements (Full Salzach*/ section of interest**)
Grain sizes	d_i [mm]	0.5, 2.0, 8.0, 16.0, 31.5, 63.0, 90.0, 140.0	Eight grain size classes in use $(i = 1,...,8)$
Grain roughness	$k'_{St,j}[m^{1/3}s{-}^{1}]$	29.6*/25.0**	Weighted average over mesh elements (Full Salzach*/ section of interest**)
Critical Shields parameter	θ_{crit} [-]	0.04	Global parameter
	Elements used for weighted average calculation: *1,525 and **950		

Table 3
Calibration Parameters and Their Range of Investigation

Calibration parameters		Investigated range		Prior assumption
Critical Shields parameter	θ_{crit} [-]	0.033	0.047	$U(0.033,0.047)$
Grain roughness	$k'_{St,j}\left[m^{1/3}s{-}1\right]$	$k'_{St,j}-4$	$k'_{St,j}+U(-4+4)$	
Grain size distribution	d_i [mm]	$d_i-0.2$	d_i+4	$d_i+U(-0.2,+4)$

and $d_i+\omega_d$ for the critical Shields parameter, grain roughness and grain size distribution. Table 3 contains the three selected parameters, their investigated range of variation, and the prior assumptions for Bayesian model calibration.

2.6. Stochastic Model Inversion

We incorporate fully Bayesian principles and perform parameter inference using the measured riverbed geometry from the years 2002, 2005, 2010, and 2013 denoted as Z_{meas}. As our prior knowledge on the uncertain calibration parameters (θ_{crit}, $k'_{St,j}$, d_i), we consider the prior probability density functions (PDF) according to Table 3. According to the Bayesian approach, given the prior knowledge and the measured data Z_{meas}, we calculate the posterior probability distribution, which is typically narrower than the prior distributions (Box & Tiao, 1973). Following the Bayesian theorem, the matching of the outputs of the sediment transport model Z (these are dependent on a set of selected calibration parameters ω) to the available measurement data Z_{meas} will be done in the following way:

$$p\left(\omega|Z_{meas}\right)=\frac{p\left(Z_{meas}|\omega\right)\,p(\omega)}{p(Z_{meas})} \tag{1}$$

where $\omega=\{\omega_{\theta_{crit}},\,\omega_{k'_{St}},\,\omega_d\}$ denotes the vector of the calibration parameters, $p(\omega)$ is their prior PDF, $p(Z_{meas}|\omega)$ represents the likelihood function of Z_{meas} given ω, $p(\omega|Z_{meas})$ is the posterior PDF of the unknown parameters and $p(Z_{meas})$ is the so-called Bayesian model evidence.

Bayesian model evidence quantifies the likelihood of a model producing the observed data averaged over the complete prior parameter space Ω with PDF $p(\omega)$ (Kass & Raftery, 1995). For this reason, Bayesian model evidence is often used as a rigorous selection or ranking criterion among competing physical models (Mohammadi et al., 2018; Wöhling et al., 2015). The present study is based on one formulation of the physical model, and hence, Bayesian model evidence will merely be considered as a normalizing constant that can be computed using the following equation:

$$p(Z_{meas})=\int_{\Omega}p(Z_{meas}|\omega)\;p(\omega)\;\mathrm{d}\omega \tag{2}$$

However, as it is merely a fixed constant for our case with a single model and a given data set, it will be irrelevant in the following (more details about model selection can be found in, e.g., Mohammadi et al., 2018). Assuming that the measurement errors ϵ between Z_{meas} and the true river evaluations are independent and Gaussian distributed, the likelihood function $p(Z_{meas}|\omega)$ is given as

$$p(Z_{meas}|\omega)=(2\pi)^{-n/2}|\mathbf{R}|^{-\frac{1}{2}}\exp\left[-\frac{1}{2}(Z_{meas}-Z(x,y,t,\omega))^{T}\mathbf{R}^{-1}(Z_{meas}-Z(x,\,y,\,t,\,\omega))\right] \tag{3}$$

where $\mathbf{R}$ is the diagonal (co)variance matrix of size $n\times n$. It represents the uncertainty in data as measured and preprocessed (i.e., interpolation of measured data on 2-D mesh). The vector Z_{meas} contains all the information available in the measured data in the calibration nodes (i.e., the nodes at the cross sections with measured data) and $n=204$ refers to the length of the observation data set Z_{meas}.

2.7. Surrogate Model via Arbitrary Polynomial Chaos Expansion

The current study focuses on a very computationally demanding, large-scale morphodynamic sediment transport model of the Lower River Salzach. Therefore, a direct implementation of Bayes theorem in Equation 1 is not feasible using any version of Monte Carlo (MC) simulation and could not even be realized via a Markov Chain Monte Carlo approach. Therefore, we alleviate this strong computational limitation by constructing a surrogate model to replicate the behavior of the original, complex morphodynamic model for the three selected calibration parameters. Referring to a recent benchmark comparison study by Köppel et al. (2019), we construct the surrogate model using the arbitrary polynomial chaos expansion technique (aPC) introduced in Oladyshkin and Nowak (2012).

The data-driven aPC approach can be seen as a machine learning approach which approximates the model output by its dependence on model parameters via multivariate polynomials. It can be interpreted as a high-order extension of first-order second-moments approaches, where higher-order statistical moments beyond mean and variance are considered (Oladyshkin & Nowak, 2018). Compared to the original polynomial chaos expansion introduced by Wiener (1938) and later extensions by Xiu and Karniadakis (2002), the aPC offers complete flexibility in the choice and representation of probability distributions. Generally, it can be seen as a mathematically optimal method for constructing a polynomial surrogate model in the range of the prior parameter distribution. By reducing the morphodynamic sediment transport model into a surrogate model based on selected calibration parameters, the method makes it possible to perform a fully blown stochastic analysis at a much faster speed.

We assume that the model parameters are distributed according to Table 3. For the purpose of surrogate modeling, the model Z can be expressed as a function $Z(x, y, t, \omega)$ of the modeling parameters $\omega = \{\omega_{\theta_{\text{crit}}}, \omega_{k_{\text{St}}'}, \omega_d\}$, and physical space x,y,t. The influence of all modeling parameters on the model output Z can be expressed as the following multivariate polynomial expansion:

$$Z(x, y, t, \omega) \approx \widetilde{Z}(x, y, t, \omega) = \sum_{i=1}^{P} c_i(x, y, t)\boldsymbol{\phi}_i(\omega) \tag{4}$$

The full model $Z(x, y, t, \omega)$ is approximated by a surrogate model $\widetilde{Z}(x, y, t, \omega)$ in Equation 4 using the expansion coefficients $c_i(x,y,t)$. The polynomials $\boldsymbol{\phi}_i(\boldsymbol{\omega})$ follow, according to polynomial chaos expansion theory, directly from the prior distributions of the selected parameters on an orthonormal basis (Oladyshkin & Nowak, 2012). The surrogate model in Equation 4 is truncated at a finite number P. This number P depends on the total number of input parameters N and on the largest considered degree of the polynomials d_p as $P = (N + d_p)!/(N!d_p)$.

The expansion coefficients $c_i(x,y,t)$ quantify the dependence of the model output on the set of modeling parameters and have to be obtained for every desired point in space and time. There are several approaches for obtaining the expansion coefficients. For practical applications, nonintrusive approaches such as the Probabilistic Collocation Method (PCM) have been receiving major attention during the last years due to their low computational cost (Webster et al., 1996). The advantage of nonintrusive methods is that they can be applied in models with high complexity and do not demand any modification of the original code (Loeven et al., 2007; Oladyshkin et al., 2011). PCM uses so-called collocation points. Collocation points are those sets of parameters $\boldsymbol{\omega}$ for which the original model is run in order to find the coefficients c_i. The selection of collocation points strongly influences the performance of the expansion in Equation 4 and dictates the number of runs needed with the expensive original model. Hence, we will follow the optimal integration theory and choose the collocation points according to the roots of the polynomial one degree higher than the order of expansion (Villadsen & Michelsen, 1978). Overall, the collocation points can be seen as given N-dimensional sets of parameters ω_i where $i = \{1, 2, \ldots, P\}$, and where the number of selected collocation points is equal to the number P of unknown coefficients c_i. Once the collocation points have been computed according to the considered prior distribution, the expansion coefficients are estimated from the following matrix equation:

$$\boldsymbol{\phi}(\omega) \times \mathbf{V}_c(x, y, t) = \mathbf{V}_Z(x, y, t, \omega) \tag{5}$$

where $\boldsymbol{\phi}(\omega)$ is the $P \times P$ matrix containing the polynomials evaluated at the P collocation points, $\mathbf{V}_c(x,y,t)$ is

the $P \times 1$ vector containing the unknown expansion coefficients c_i for each location (x, y) and time step t, and $\mathbf{V}_Z(x, y, t, \omega)$ is a $P \times 1$ vector that contains the model outputs of the original model $Z(x, y, t, \omega_i)$ evaluated for each of the P collocation points ω_i. The matrix $\phi(\omega)$ is time and space independent, meaning that it can be generated once for a given expansion degree and number of calibration parameters. On the other hand, the vectors $\mathbf{V}_c(x, y, t)$ and $\mathbf{V}_Z(x, y, t, \omega)$ are time and space dependent, which means that they have to be obtained for each location (x, y) and time step t. Once the expansion coefficients c_i have been calculated from Equation 5, we have constructed the surrogate model $\widetilde{Z}(x, y, t, \omega)$ in Equation 4. Technically, the expansion coefficients of the polynomials c_i are calculated for each node n in the mesh and for each calibration (and validation) time step t.

2.8. Iterative Bayesian Updating of the Surrogate Model

To perform Bayesian updating, we replace the response from the original morphodynamic sediment transport model $Z(x, y, t, \omega)$ in the likelihood Equation 3 by its surrogate $\widetilde{Z}(x, y, t, \omega)$:

$$p(Z_{\text{meas}}|\omega_k) \propto exp\left[-\frac{1}{2}\left(\widetilde{Z}(x,y,t,\omega_k)-Z_{\text{meas}}\right)^T \; R^{-1} \; \left(\widetilde{Z}(x, y, t, \omega_k) - Z_{\text{meas}}\right)\right] \tag{6}$$

Then, we draw a large number of Monte Carlo samples ω_k with $k = 1,...,100{,}000$ according to the considered prior distributions of ω. Subsequently, we evaluate the surrogate model $\widetilde{Z}(x, y, t, \omega)$ for each Monte Carlo parameter combination ω_k and use the measured data of riverbed geometry (Z_{meas}) in Equation 6 to approximate the corresponding likelihoods.

The surrogate model may, however, be imprecise and may produce incorrect outcomes in the parameter ranges that show high likelihood because all approaches based on polynomial chaos expansion want to have the smallest possible squared error on average over the prior, but not over the posterior (Oladyshkin & Nowak, 2012). To overcome this issue, we employ an iterative Bayesian updating process that improves the accuracy of the surrogate model by incorporating new collocation points ω_{new} corresponding to the maximum a posteriori (MAP) value (Oladyshkin, Class, et al., 2013). In other words, we compare each realization $\widetilde{Z}(x, y, t, \omega_k)$ (i.e., riverbed elevations) with the measured data Z_{meas} and identify the MAP. Thus, each iteration suggests a new collocation point at which we run the full morphodynamic model to assess the outcome $Z(x, y, t, \omega_{\text{new}})$. Then, we update the expansion coefficients by solving Equation 5, which is now an overdetermined system and becomes a least square scollocation problem (Moritz, 1978). Through this procedure, we iteratively obtain a surrogate model that contains more accurate information about the model in all alleged regions of interest where the likelihood to capture the data is higher. As stopping criterion for this iteration, we repeat until the current posterior distribution shows only minor changes in comparison to the previous one, indicating convergence.

We can afford a plain rejection sampling technique to estimate the posterior distribution $p(\omega|Z_{\text{meas}})$ at each iteration step. We use the rejection sampling method (Smith & Gelfand, 1992) because the surrogate model is cheaper to evaluate, and so allows drawing a large number of parameter combinations ω_k with $k = 1, ...,100{,}000$ from the prior distributions and the evaluation of the surrogate model output $\widetilde{Z}(x, y, t, \omega_k)$ for each set of ω_k. Rejection sampling represents the posterior distribution according to the following importance weights W_k:

$$W_k = \frac{p(Z_{\text{meas}}|\omega_k)}{\max\ (p(Z_{\text{meas}}|\omega_k))} \tag{7}$$

Importance weights W_k are the probabilities of accepting prior realizations as posterior realizations; all other ones are rejected. A realization ω_k is accepted when $W_k \geq U_k$, where U_k is a random number drawn from the uniform distribution $U(0,1)$, and otherwise rejected.

2.9. Assessing the Quality of Bayesian Calibration and Validation

Monte Carlo simulations of the aPC iterative Bayesian updating process estimate the prior and the posterior distribution of the model output. From this, we compute the expected riverbed evolution for the entire Lower River Salzach. Standard deviations from these expected values and also the MAP estimate are

available. In this case, with a uniform prior distribution, the MAP estimate is the realization of the Monte Carlo sample with the highest likelihood value (Equation 6) and corresponds to the deterministic best fit solution. The MAP can thus be compared to the parameter combination found during conventional (i.e., manual) calibration. To display the morphodynamic development (riverbed evolution) for calibration (2002–2010) and validation (2010–2013), we roll out the mean value $\langle \Delta \widetilde{Z} \rangle (x,y,t,\omega_k)$ of the aPC model results on the entire movable riverbed in the section of interest, that is, at the nodes of the original mesh ($n = 1{,}138$). $\langle \Delta \widetilde{Z} \rangle_{n,t}$ is calculated for a particular node n and time step t by considering the measured riverbed elevation Z_{meas} from the year 2002 (calibration) or 2010 (validation) as initial riverbed:

$$\langle \Delta \widetilde{Z} \rangle_{n,t} = \frac{\sum_{k=1}^{S} \widetilde{Z_k}}{S} - Z_{2002,2010} \tag{8}$$

where $\widetilde{Z}$ is the corresponding aPC model output for a combination ω_k taken from the prior PDFs or for an accepted combination ω_k taken from the posterior PDFs. The sample size is represented by S (for example 100,000 in the prior simulations). Subsequently, we derive statistical quantities and estimate the spatial mean and the spatial standard deviation of the riverbed evolution. With this, we can evaluate and quantify the prior and posterior uncertainties and assess the quality of Bayesian calibration and validation.

2.10. Verification of Surrogate Model

The aPC results are verified against the results of the original morphodynamic model to test the approximation made by Equation 4. For this purpose, we compute the root-mean-square error ϵ between the outputs $\Delta \widetilde{Z}_{n,t}$ of the surrogate model and the outputs $\Delta Z_{n,t}$ of the original model obtained with the MAP parameter combination ω_{MAP} as follows:

$$\epsilon = \sqrt{\frac{1}{n} \sum_{i=1}^{n} \left(\Delta Z_{n,t}(\omega_{\text{MAP}}) - \Delta \widetilde{Z}_{n,t}(\omega_{\text{MAP}}) \right)^2} \tag{9}$$

2.11. Validation of Model Results and Comparison to the Earlier Manual Calibration

As a final step, we calculate the residuals between the measured and simulated riverbed evolution for each calibration node ($n = 204$) as follows:

$$e = \Delta Z_{\text{meas}} - \left\{ \begin{matrix} \Delta Z_{n,t} \\ \Delta \widetilde{Z}_{n,t}(\omega_{\text{MAP}}) \\ \Delta Z_{n,t}(\omega_{\text{MAP}}) \end{matrix} \right\} \tag{10}$$

where ΔZ_{meas} is a vector that contains the measured riverbed evolution, $\Delta Z_{n,t}$ contains the results of the manually calibrated full model, and $\widetilde{Z}_{n,t}(\omega_{\text{MAP}})$ and $Z_{n,t}(\omega_{\text{MAP}})$ contain the results of the surrogate and the full model obtained with the ω_{MAP} parameter set, respectively.

In doing so, we are able to derive the distribution of the residuals e for the calibration (2002–2010) and validation (2010–2013) period as well as the corresponding statistical quantities, that is, mean error ($\bar{e}$), standard deviation (σ_e) and root-mean-square error (ϵ_e). Consequently, we can assess the overall quality of the stochastically calibrated models and eventually relate our findings to the previously manually calibrated full complex model.

3. Results and Discussion of the Bayesian Calibration and Validation of the Sediment Transport Model

3.1. Iterative Bayesian Updating of the Surrogate Model

We construct a surrogate model using a second-order aPC expansion according to the prior distributions of the calibration parameters $\omega = \{\omega_{\theta_{\text{crit}}}, \omega_{k_{\text{St}}'}, \omega_d\}$ (Table 3). For this purpose, the surrogate model requires the model output $Z(x, y, t, \omega)$ of the original morphodynamic sediment transport model obtained for the parameter combinations defined by 10 collocation points. Figure 2 illustrates these original collocation points

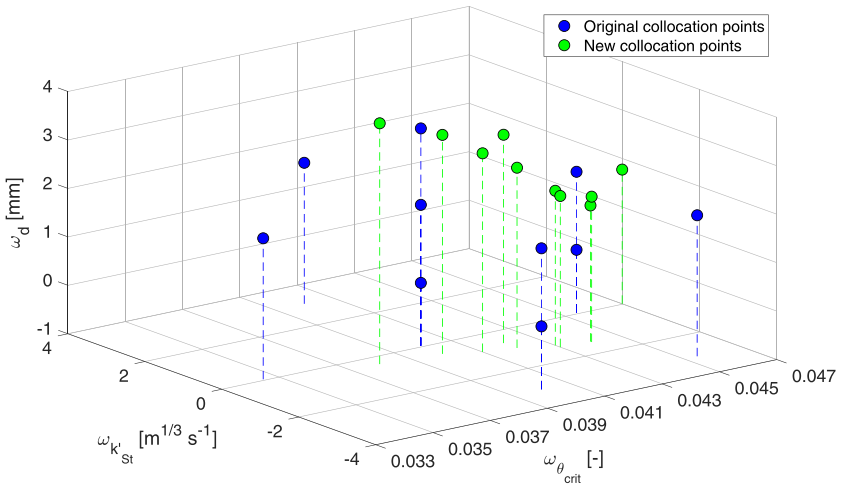

Figure 2. Representation of original collocation points for the construction of the surrogate model in the parameter space of the calibration parameters and the new collocation points obtained by iterative Bayesian updating.

within the parameter space of the calibration parameters θ_{crit}, $k'_{St,j}$, d_i. We use Equation 5 to find the aPC surrogate in Equation 4.

Figure 3 illustrates the randomly drawn combinations of parameters ω_k ($k = 1...N_{\text{MC}}$; $N_{\text{MC}} = 10^5$) occurring during the Monte Carlo procedure and the corresponding outputs from the surrogate model $\widetilde{Z}(x,\ y,\ t,\ \omega_k)$ for one exemplary node in the mesh (node id: 13,319). The color scheme indicates the values of the resulting river bed elevation $\widetilde{Z}$ at a time step $t = 2010$ (end of calibration period).

Following the Bayesian framework, each realization is weighted through the likelihood upon comparison with the measured riverbed elevation at the calibration nodes ($n = 204$) according to Equation 6. Then, we iterate according to section 2.8. Therefore, Figure 2 contains, in addition to the 10 original collocation points used to construct the zeroth-iteration surrogate model (blue dots), also 10 new collocation points obtained during the iterative Bayesian updating (green dots). The new iteratively chosen collocation points correspond to regions with higher likelihood values. The iterative Bayesian updating is successful if the posterior distributions of the calibration parameters narrowed and stabilized. This condition has been reached after 10 iteration steps. Each iteration requires approximately 4 hr of computation time (updating the aPC, computing the likelihood and rejection sampling on the 10^5 MC candidates).

Figures 4a–4d show the individual obtained posterior PDFs for the calibration parameters after the first, second, ninth, and tenth iterations. In each subfigure, the posterior combinations are sorted into 20 equally spaced bins. The vertical dashed lines indicate the values obtained via manual calibration. It can be seen that, for all three calibration parameters, the PDF has narrowed and stabilized towards the end (between the ninth and tenth iterations). However, in the univariate views of Figures 4a–4d, it is not easy to see that the calibrated parameters have a strong nonlinear dependence on each other. To visualize this nonlinear dependence, we plot in Figure 5 the importance weights W_k in a multivariate scatter plot after the tenth iteration of Bayesian updating. Parameter combinations with likelihood values near zero are not shown. The red color represents the $N = 857$ accepted (posterior) Monte Carlo samples with the highest likelihood values, that is, those that result in the most acceptable match to the measured data Z_{meas}. The maximum a posteriori (MAP) combination obtained after the tenth iteration of Bayesian updating is given in Table 4. Referring the MAP combination back to the absolute values given in Table 2, this results in an increase in critical Shields parameter from 0.04 to 0.044, a reduction in grain roughness from 25.03 m$^{1/3}$ s^{-1} to 23.69 m$^{1/3}$ s^{-1} (weighted average over all elements in the section of interest), and in an increase in the grain size classes to $d_i = \{2.13, 4.13, 10.13, 18.13, 33.63, 65.13, 92.13, 142.13\}$ mm.

Although the parameter combination with the highest likelihood can be derived (MAP), Figure 5 reveals a variety of parameter combinations resulting in a high likelihood, that is, they are all possible combinations. Thus, the outcomes demonstrate that one single deterministic solution does not exist, given the

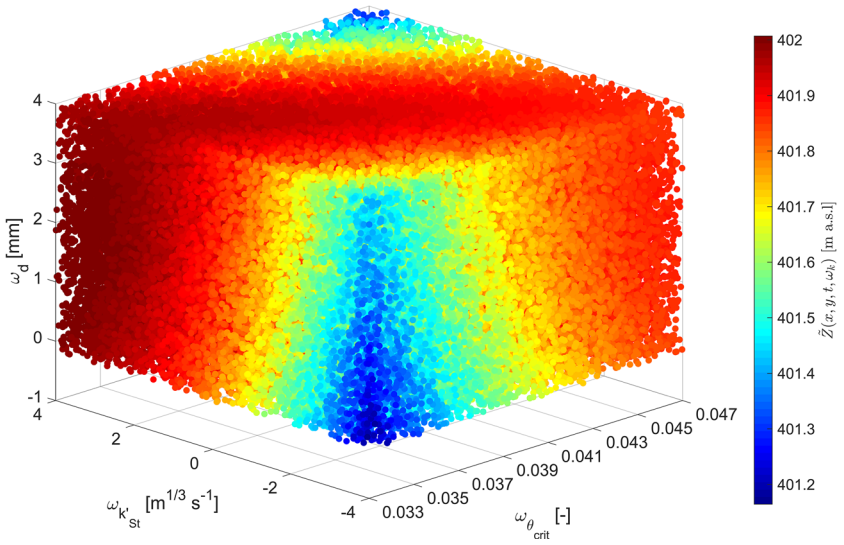

Figure 3. N_{MC} combinations ($N_{MC} = 10^5$) and surrogate model outputs $\widetilde{Z}(x, y, t, \omega_k)$ for one exemplary node in the mesh (node id: 13,319) and the calibration time step $t = 2010$.

interdependence of the calibration parameters. This underlines the need for stochastic calibration procedures in morphodynamic sediment transport modeling since the commonly applied models are highly parameterized (e.g., Merritt et al., 2003), including multiple parameter interdependencies (e.g., the relation between grain roughness and grain size, (see Strickler, 1923) or the relation between critical shear stress and grain size (see Buffington & Montgomery, 1997)). This interdependency of the three calibration parameters is clearly reflected in Figure 5.

3.2. Bayesian Model Calibration With the Surrogate Model

Figure 6 illustrates the results of the aPC surrogate model for the calibration period (2002–2010) for the section of interest in the Lower River Salzach (km 59.3 to km 52.4). The results are separated into those obtained with the prior and posterior distributions of the considered calibration parameters. Figures 6a and 6b show the mean riverbed evolution $\langle \Delta \widetilde{Z} \rangle_{n,t}$ obtained with (a) the $N_{MC} = 100{,}000$ candidates from the prior and (b) with the $N = 857$ candidates that were accepted after rejection sampling (posterior) in the last iteration. Figures 6c and 6d show the standard deviation $\sigma_{n,t}$ among all aPC results for (c) the prior distribution and (d) the posterior distribution.

The prior and posterior mean results show a similar pattern of erosion and deposition along the Lower River Salzach, with alternating gravel bars and deepenings of up to ±3 m. However, local deviations exist, leading to a spatial mean riverbed evolution of −0.17 m in Figure 6a and −0.05 m in Figure 6b. Calibration demonstrates that there is less erosion in comparison with the prior assumptions. This can be attributed to the updated posterior parameter sets, in which θ_{crit} and d_i have increased and k'_{St} has decreased (cf. Figure 5, Table 4). In the applied equation of Hunziker (1995) as well as in the original equation of Meyer-Peter and Mueller (1948), the parameters d_i and k'_{St} both appear in the denominator as part of the dimensionless bed-forming shear stress. The dimensionless bed-forming shear stress is then compared to the critical shear stress by subtracting the latter from the former value and so an increased value for θ_{crit} induces higher resistance of the riverbed towards erosion. Since erosion-mitigating effects dominate the calibration results, less erosion is the consequence.

The corresponding standard deviations of all model outputs have an average of 0.73 m in the prior (Figure 6c) and 0.15 m in the posterior results (Figure 6d). When spatially integrated, this leads to a volumetric standard deviation of 414,610 m^3 in the prior and 83,174 m^3 in the posterior. The prior results have regions with an increased prior standard deviation up to 1 m in many parts of the river. Critical spots are mainly located in the upstream section and close to the outflow. In the upstream section of the Lower River Salzach, the sediment input from the Saalach River dominates the morphodynamic behavior. The

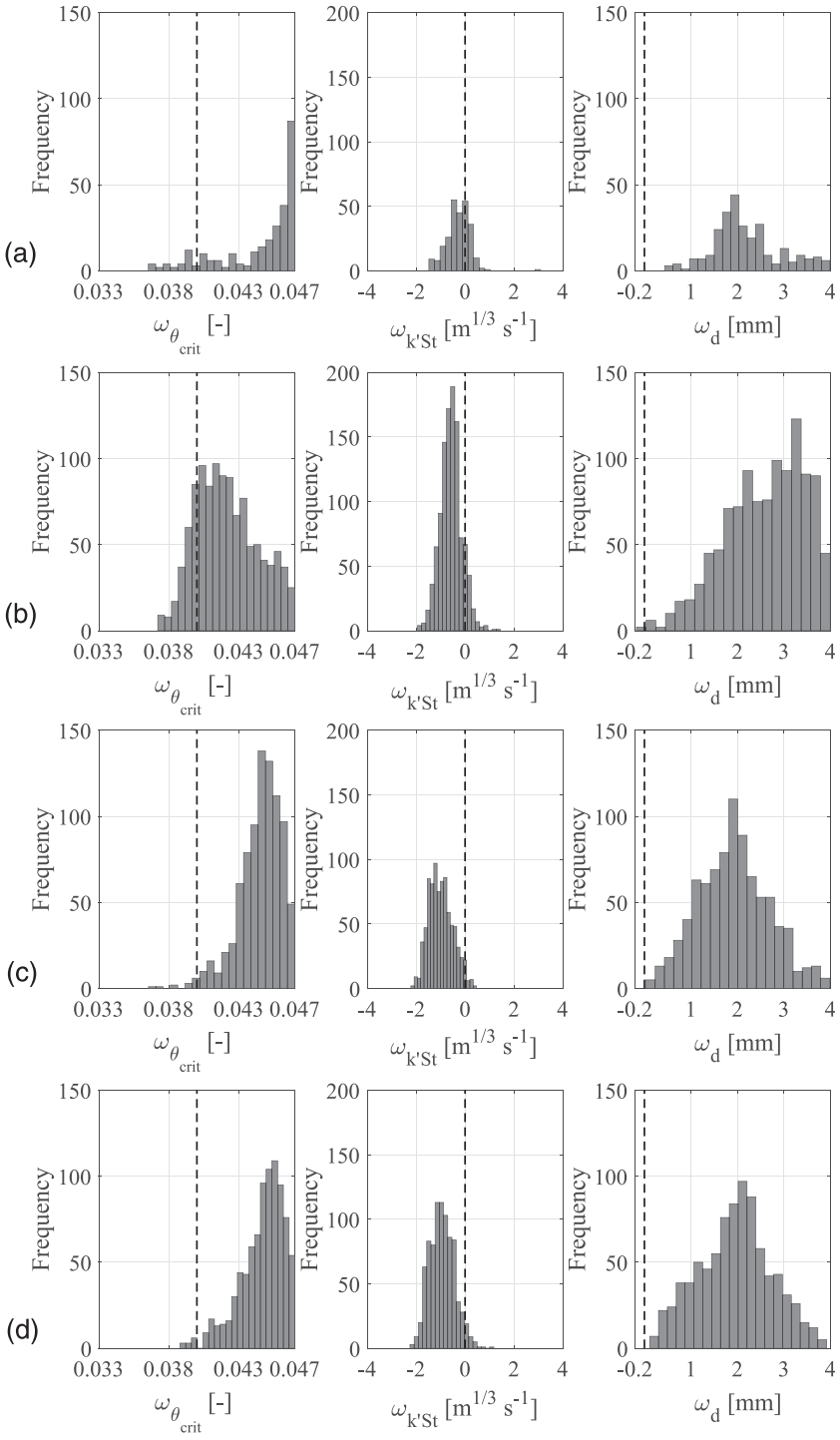

Figure 4. Posterior distributions of the three selected calibration parameters θ_{crit}, $k'_{St,j}$, and d_i during the iterative Bayesian updating obtained after (a) first iteration, (b) second iteration, (c) ninth iteration, and (d) tenth (final) iteration. The vertical dashed lines refer to the manually calibrated value.

three-dimensional effects in the mixing zone close to the confluence are highly complex, and so are affected in a nonlinear fashion and to a high degree by parametric uncertainties. In the downstream section, the effect of the lower boundary condition impacts the prior results, explaining the uncertainties in the prior simulations. When looking at the posterior standard deviation obtained with the calibrated posterior

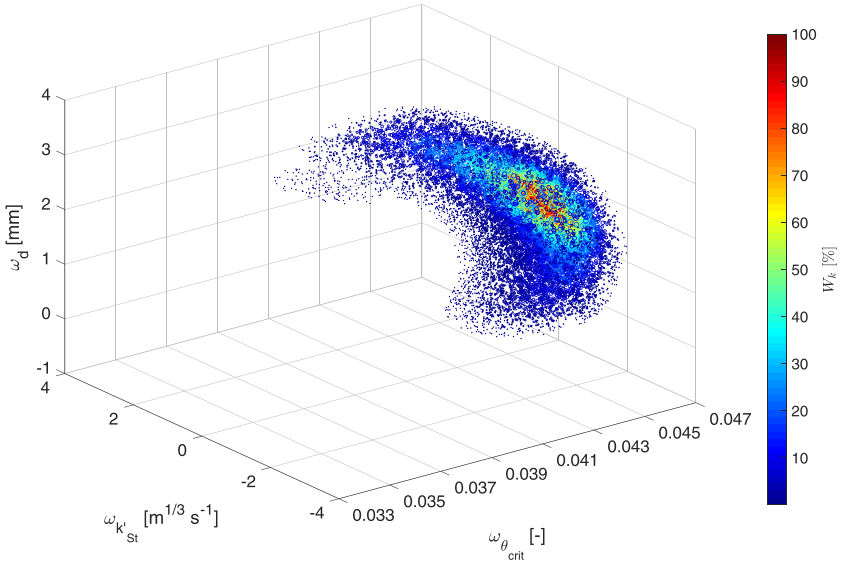

Figure 5. Likelihood dependency of the three calibration parameters after the tenth Bayesian update.

parameter distributions (Figure 6d), it can be seen that the uncertainties have significantly decreased. This can be quantified by the decrease in the mean spatial standard deviation of 0.58 m (331,436 m^3). Thus, the posterior parameter distributions obtained from Bayesian updating have significantly increased the quality of the aPC surrogate model. Only a few remaining spots, again close to the edges of the model domain, show higher remaining uncertainties. The remaining (now reduced) uncertainties indicate that the Bayesian calibration revealed a spread of simulations with well-fitting solutions. Vice versa, it implies that a manually obtained deterministic calibration lacks robustness. This generally confirms the results of previous studies (Schmelter et al., 2011, 2012; Schmelter & Stevens, 2013) and emphasizes the significant contribution of Bayesian updating in morphodynamic and sedimentological studies to capture more accurately and realistically the underlying processes (Mohammadi et al., 2018; Wu & Chen, 2009).

3.3. Results of the Surrogate Model for the Validation Period

We validate the distribution of parameter combinations found during Bayesian calibration with an independent set of measured data from the year 2010 to 2013. Figure 7 illustrates the results of the aPC surrogate model for the validation period (2010–2013) along the section of interest in the Lower River Salzach. The results are again separated into those obtained with the prior and posterior distributions. Figures 7a and 7b show the mean riverbed evolution $\langle \Delta \widetilde{Z} \rangle_{n,t}$ obtained with (a) the prior and (b) the posterior parameter distribution.

Table 4
Maximum a Posteriori (MAP) Set of Parameter Combinations Found During Bayesian Updating of the aPC Surrogate Model

Calibration parameters		Prior assumption	Maximum a posteriori (MAP)
Critical Shields parameter	θ_{crit} [-]	$U(0.033,0.047)$	0.044
Grain roughness	$k'_{St,j}\left[m^{1/3}s^{-}\right]$	$k'_{St,j}+U(-4\,,+4)$	$k'_{St,j}-1.34$
Grain size distribution	d_i [mm]	$d_i+U(-0.2,+4)$	$d_i+2.13$

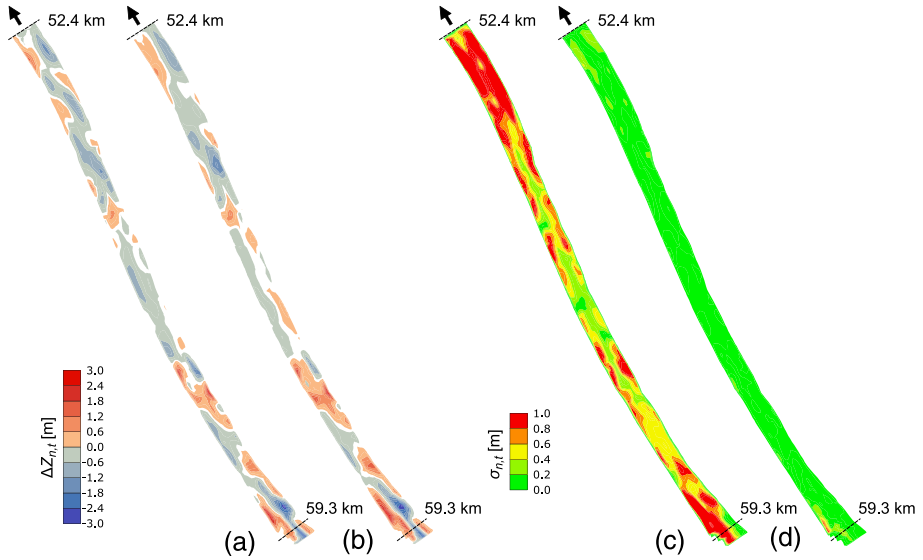

Figure 6. Simulated riverbed evolution ($\langle \Delta \widetilde{Z} \rangle_{n,t}$) obtained with the aPC surrogate model in the Lower River Salzach (km 59.3 to km 52.4) for the calibration period (2002–2010) and the corresponding standard deviation ($\langle \sigma \rangle_{n,t}$): (a) prior mean result, (b) posterior mean result, (c) prior standard deviation, and (d) posterior standard deviation. Please note that the river width is artificially stretched by a factor of 3; white regions indicate no riverbed change.

The prior and posterior mean results show a similar pattern for the simulated riverbed morphology. Alternating gravel bars and deepenings are clearly visible along the Lower River Salzach. Deviations are present in the downstream and upstream section. The corresponding spatial mean is −0.03 m for Figure 7a and −0.02 m for Figure 7b. The similar values can be explained by the overall decreased magnitude of erosion and deposition in the posterior results, leading on average to almost the same net evolution. Figures 7c and 7d show the standard deviation $\sigma_{n,t}$ among all aPC results obtained from (c) the prior and (d) the posterior distribution. The corresponding spatial mean now decreased from 0.67 to 0.15 m. When spatially integrated, this results in a volumetric reduction from 379,043 m^3 in the prior to 86,408 m^3 in the

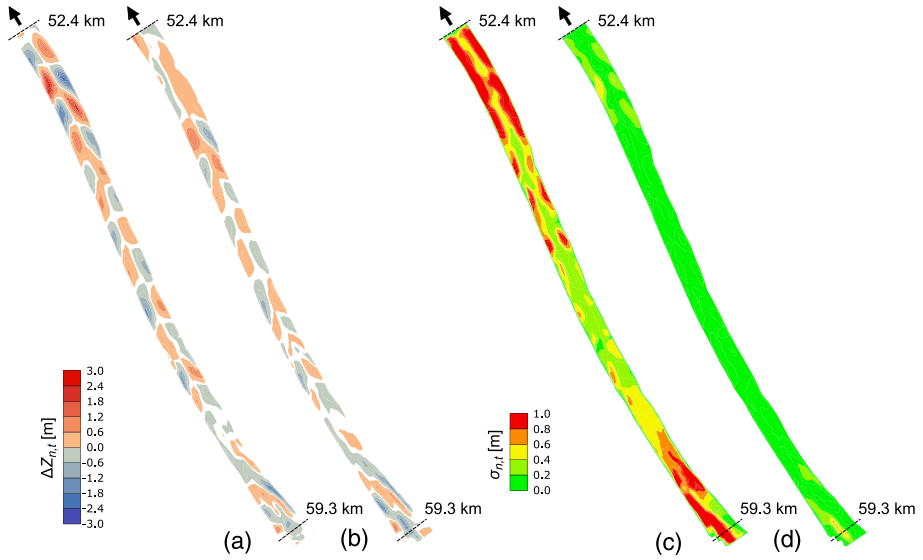

Figure 7. Simulated riverbed evolution ($\langle \Delta \widetilde{Z} \rangle_{n,t}$) obtained with the aPC surrogate model in the Lower River Salzach (km 59.3 to km 52.4) for the validation period (2010–2013) and the corresponding standard deviation ($\langle \sigma \rangle_{n,t}$): (a) prior mean result, (b) posterior mean result, (c) prior standard deviation, and (d) posterior standard deviation. Please note that the river width is artificially stretched by a factor of 3; white regions indicate no riverbed change.

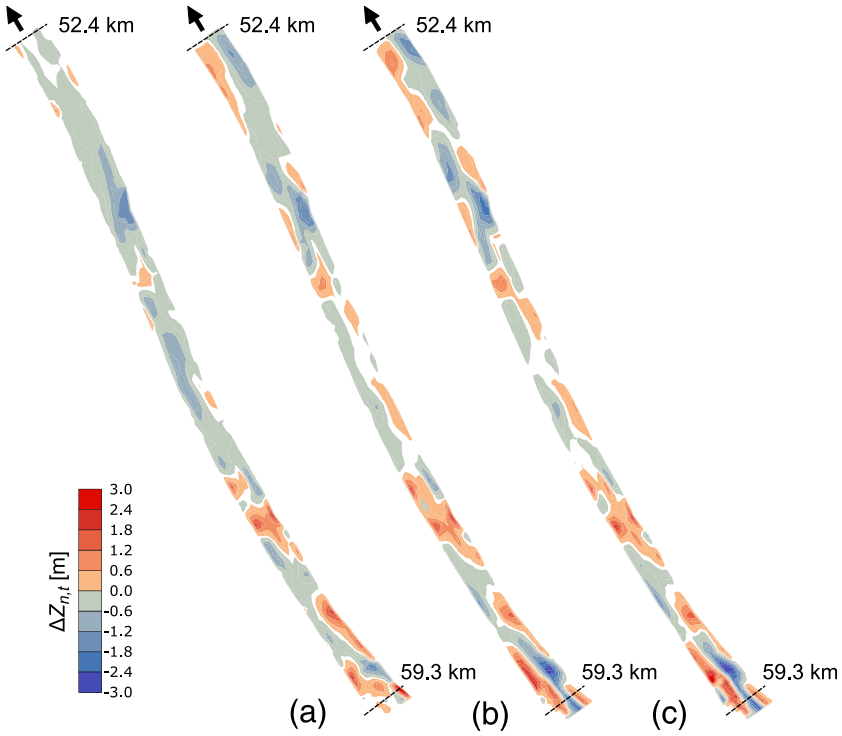

Figure 8. Riverbed evolution in the Lower River Salzach (km 59.3 to km 52.4) for the calibration period 2002–2010 obtained from (a) measurements, (b) stochastically calibrated aPC surrogate model (MAP), and (c) stochastically calibrated morphodynamic model (MAP). Please note that the river width is artificially stretched by a factor of 3; white regions indicate no riverbed change.

posterior. It can be concluded, that the posterior parameter combinations found during Bayesian calibration also increase model quality and robustness for an independent set of data. Thus, we rate the validation with the surrogate model as successful.

3.4. Verification of the Surrogate Against the Full Sediment Transport Model

In order to verify the aPC surrogate model, we apply the maximum a posteriori (MAP) set of calibration parameters obtained from the tenth Bayesian iteration (see Table 4) to both, the surrogate and the original *Hydro_FT−2D* sediment transport model. The results obtained with this parameter set for calibration and validation can be interpreted as the best deterministic scenario simulated with the aPC surrogate model and with the original morphodynamic sediment transport model.

Figure 8 shows the resulting riverbed evolution for the calibration period (2002–2010). Figure 8a contains the measured riverbed evolution (only important in section 3.5), Figure 8b the riverbed evolution simulated with the surrogate model ($\Delta\widetilde{Z}_{n,t}(\omega_{\mathrm{MAP}})$) and Figure 8c the corresponding riverbed evolution simulated with the full morphodynamic model ($\Delta Z_{n,t}(\omega_{\mathrm{MAP}})$). As expected, the simulation result of the aPC surrogate model (Figure 8b) shows very good agreement with the simulated riverbed evolution of the full morphodynamic model (Figure 8c). This is due to the iterative Bayesian updating process to improve the surrogate. The root-mean-square error between the two models results in $\epsilon_{\mathrm{Cal}} = 0.31$ m.

Figure 9 shows the riverbed evolution for the validation period (2010–2013). Figure 9a contains the measured riverbed evolution (only important in section 3.5), Figure 9b the riverbed evolution simulated with the aPC surrogate model ($\Delta\widetilde{Z}_{n,t}(\omega_{\mathrm{MAP}})$), and Figure 9c the corresponding riverbed evolution obtained with the morphodynamic model ($\Delta Z_{n,t}(\omega_{\mathrm{MAP}})$) using the MAP set of parameters and being initialized from the simulated river bed morphology of the calibration period. Again, the simulated riverbed evolution of the aPC surrogate model (Figure 9b) shows very good agreement with the riverbed evolution simulated with

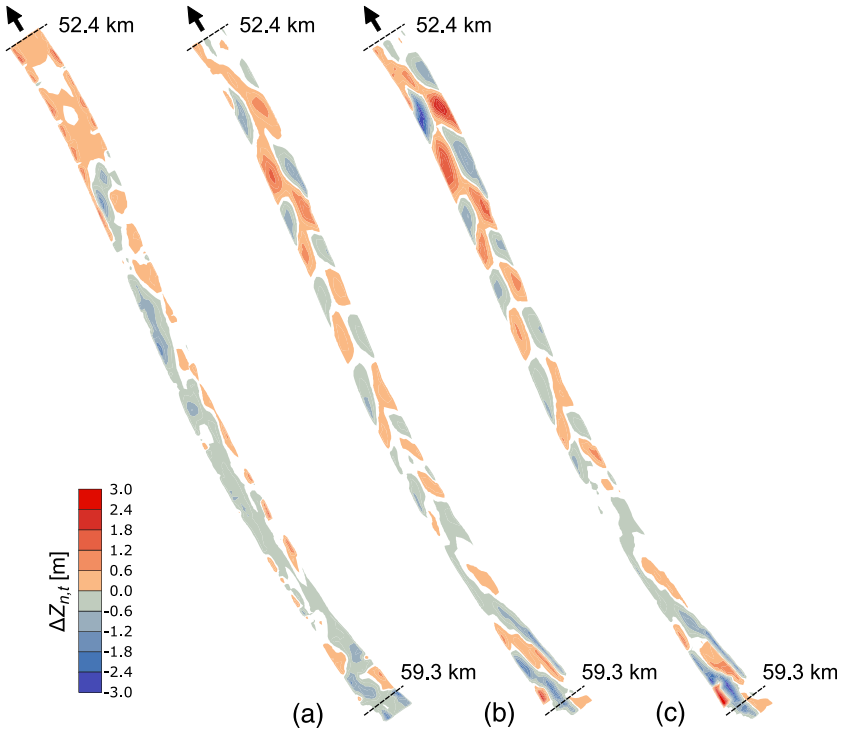

Figure 9. Riverbed evolution in the Lower River Salzach (km 59.3 to km 52.4) for the validation period 2010–2013 obtained from (a) measurements, (b) stochastically calibrated aPC surrogate model (MAP), and (c) stochastically calibrated morphodynamic model (MAP). Please note that the river width is artificially stretched by a factor of 3; white regions indicate no riverbed change.

the original morphodynamic model (Figure 9c). The root-mean-square error between the two models is $\epsilon_{\mathrm{Val}} = 0.42$ m.

Model verification by means of the root-mean-square error indicates that our constructed aPC surrogate model approximates in a reliable manner the fully deterministic sediment transport model ($\epsilon_{\mathrm{Cal}} = 0.31$ m and $\epsilon_{\mathrm{Val}} = 0.42$ m). Although a performance loss is seen from calibration to validation, this is a typical degree and not to be blamed on the surrogate. The aPC surrogate model can thus be used to study the complex morphodynamic behavior in the Lower River Salzach since the data fit for calibration and validation is of very good quality (Figures 8b, 8c, 9b, and 9c).

3.5. Validation and Comparison to the Earlier Manual Calibration

Now we look again at Figures 8 and 9. The simulations conducted with the stochastically calibrated models (Figures 8b and 8c) reproduce well the measured evolution pattern of the calibration period (Figure 8a). Deviations are visible in the upstream section close to the Saalach confluence where the simulated evolution amplitude is increased and in the downstream section where the simulations underestimate the measured riverbed erosion and predict emerging gravel bars. The riverbed evolution measurements for the validation period (Figure 9a) are less accurately reproduced by both models since the evolution amplitude close to the Saalach confluence is still increased and gravel bars clearly emerge in the downstream section of the Lower River Salzach (Figures 9b and 9c). Moreover, the measurements in vicinity of the outflow indicate low but wide deposition. This is not reflected in the simulation results as they also predict progressing gravel bars for this region. A general observation of the measured evolution pattern indicates, however, a trend toward deposition and an existence of gravel bars in the section of interest. It should be further noted, that the largest deviations occur in regions where the highest uncertainties can be found. These uncertainties, however, remain significantly reduced through Bayesian calibration (Figure 6 and 7). Nevertheless, it is likely that both models overestimate the river dynamics in the Lower River Salzach. We attribute this to the numerical implementation of the sediment input from the River Saalach in the full morphodynamic model. Although the total volumes are well documented, the intermittent character that stems from the operation

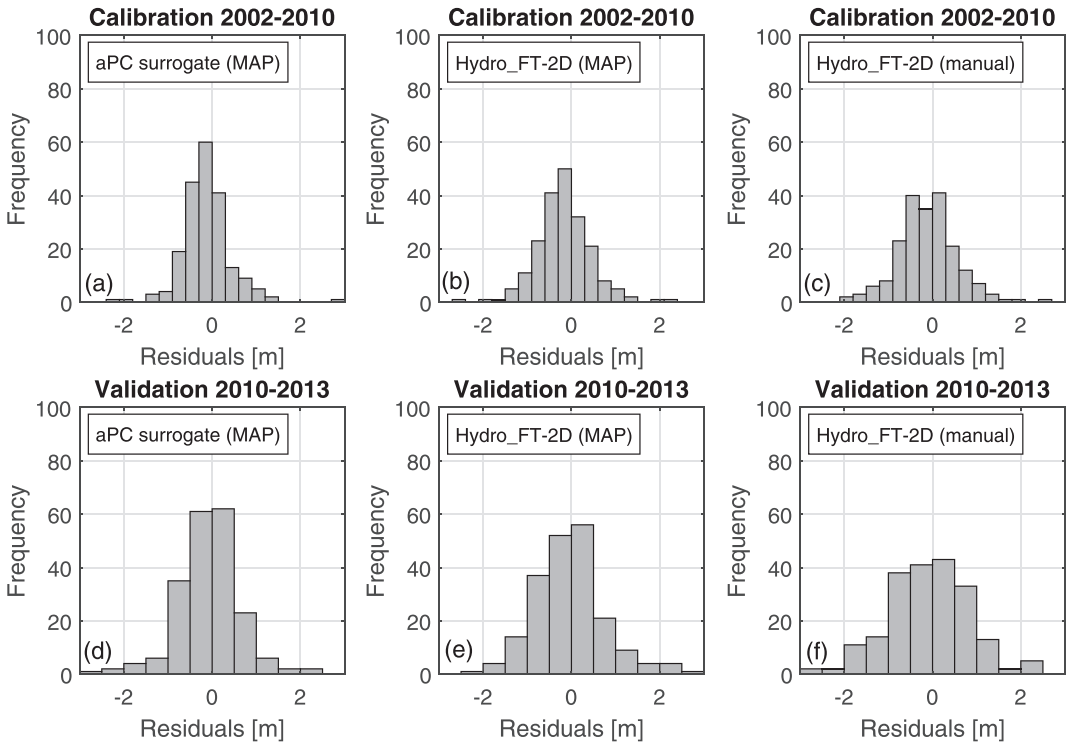

Figure 10. Comparison of differently calibrated models by means of a residual analysis showing the difference between the measured and simulated riverbed evolution for all calibration nodes ($n = 204$). The upper panels contain the results for the calibration period (2002–2010) whereas the lower panels contain the results for the validation period (2010–2013).

of a hydroelectric power plant and respective flushing events (Beckers et al., 2018) cannot be accurately approximated with the river-specific rating curve used in the full model (Beckers et al., 2016, 2018). Instead, the more continuous sediment supply due to the rating curve applied resembles the historic condition of the Lower River Salzach with distinct gravel bars moving down the river. From a 2-D numerical perspective, it is also conceivable that the full model might underestimate transverse bed slope effects on sediment transport. In general, the effect and consideration of slope effects in 2-D models are widely discussed (e.g., Recking, 2009; Siviglia et al., 2013). More specifically, for a braided river it has been shown that an underestimation of transverse bed slope effects may cause an overestimation of river dynamics and results in deeper/narrower channels (Williams et al., 2016). Consequently, the aPC surrogate model cannot capture these effects either as it was built based on the full complex morphodynamic model (Equation 4). Further studies that test the sensitivity of transverse bed slope effects on sediment transport and focus in particular on possibilities to optimize the sediment input numerically using the full complex morphodynamic model in combination with problem-based surrogates are thus recommended.

Table 5
Statistical Quantities of Residuals e Obtained for Differently Calibrated Models Divided Into Mean Error ($\bar{e}$), Standard Deviation (σ_e) and Root-Mean-Square Error (ϵ_e)

Period	Model and calibration strategy	$\bar{e}$ [m]	σ_e [m]	ϵ_e [m]
Calibration (2002–2010)	aPC surrogate (MAP)	−0.14	0.54	0.56
	Hydro_FT-2D (MAP)	−0.15	0.67	0.68
	Hydro_FT-2D (manual)	−0.11	0.67	0.68
Validation (2010–2013)	aPC surrogate (MAP)	−0.08	0.69	0.70
	Hydro_FT-2D (MAP)	−0.06	0.88	0.88
	Hydro_FT-2D (manual)	−0.08	0.91	0.91

Note. The full distribution is given in Figure 10.

In a final step, we carry out a residual analysis to assess the overall quality of the models and finally compare the stochastically calibrated results using the MAP parameter combination (Table 4) with those obtained through manual calibration. The residuals e are calculated according to Equation 10 for each calibration node ($n = 204$) and their distribution is shown in Figures 10a–10f. The results for the calibration period are shown in the upper panels for (a) the stochastically calibrated aPC surrogate model (MAP), (b) the stochastically calibrated sediment transport model (MAP), and (c) the manually calibrated sediment transport model. The lower panels contain, accordingly, the results for the validation period for (d) the stochastically calibrated aPC surrogate model (MAP), (e) the stochastically calibrated sediment transport model (MAP), and (f) the

manually calibrated sediment transport model. Table 5 presents the corresponding statistical quantities of the residuals.

The distributions of the residuals for calibration (2002–2010) and validation period (2010–2013) suggest an improvement of the stochastically calibrated surrogate (Figures 10a and 10d) over the stochastically calibrated full model (Figure 10b and 10e) to the manually calibrated morphodynamic model (Figure 10c and 10f). This ranking is confirmed by the statistical quantities and the root-mean-square errors ϵ_e given in Table 5. While the manually calibrated morphodynamic model performs as good as the stochastically calibrated morphodynamic model in the calibration period, the stochastically calibrated morphodynamic model outweighs the manual calibration in the validation period. This can be explained with the significantly reduced posterior uncertainty (Figures 6 and 7) and the applied maximum a posteriori (MAP) parameter combination (Table 4) resulting from Bayesian calibration. As expected, the MAP parameter combination is more robust compared to the manually calibrated parameters and thus performs better on an independent data set, that is, for the validation period.

In summary, all calibrated models (stochastic and manual) produce sufficiently accurate results when considering the total dimensions of the investigated river section (6.9 km long, on average 82 m movable riverbed width) and the limitations given by the original morphodynamic *Hydro_FT−2D* sediment transport model. Moreover, the consistent negative mean errors of the residuals (Table 4) confirm that all models overestimate the deposition in the Lower River Salzach and underline the need for future studies on the numerical implementation of the sediment input from the River Saalach.

3.6. Overall Assessment of Bayesian Calibration and Validation Using the Surrogate

It has been shown, that the stochastically calibrated full morphodynamic model has the same accuracy and performs better than the manually calibrated full morphodynamic model. However, the main difference between both calibration methods is on the computational effort required to achieve an acceptable fit with the measured riverbed evolution. While the computational effort for one run of the full morphodynamic model is 7.14 hr for calibration and 2.0 hr for validation, one call of the aPC surrogate model, now merely a polynomial, is 13.52 ms (for calibration and validation). Given this, obtaining the N_{MC} model outputs by testing 100,000 parameter combinations requires 0.38 hr. Considering that the aPC surrogate model was constructed with 20 runs of the full complex morphodynamic model (definition of initial and updated collocation points) and required ∼4 hr for each of the 10 iterations (Gaussian likelihood and rejection sampling of the 100,000 MC candidates) during Bayesian calibration, ∼222.8 hr are required to obtain the final accepted parameter combination. During manual calibration, more than 200 parameter combinations were tested with the full morphodynamic model (Beckers et al., 2016, 2018). This corresponds to approximately 1,828 hr of computation time. In terms of total time requirement, the final accepted parameter combination, that is, the maximum a posteriori (MAP) combination, was obtained via Bayesian calibration in about one-eighth of the time compared to the manual calibration. This result makes clear the significant time reduction.

For the presented case, we could define three most sensitive parameters based on the previous conducted numerical studies on the Lower River Salzach. In the event that more calibration parameters shall be considered during stochastic calibration, the total computational time scales solely with the additionally required full model runs to define the collocation points to construct the surrogate (Equation 4). An increase to four or five parameters leads to 15 or 21 full model runs for constructing the initial aPC surrogate, respectively. Using the evidence from this study, the same number of iterations (Bayesian updating of the surrogate against measured data) is approximately required to refine the surrogate. This leads to 15 and 21 supplementary full model runs to find the new collocation points. Therefore, the total time requirement would result in 314.2 hr (four calibration parameters) and 423.9 hr (five calibration parameters) and indicates roughly a linear increase in time for each additionally considered calibration parameter.

4. Summary and Conclusions

The presented work provides a stochastic calibration and validation for a morphodynamic sediment transport model of the Lower River Salzach. A Bayesian framework is employed with a surrogate model constructed via arbitrary polynomial chaos expansion (aPC). Considering the strong computational limitations of the physical-deterministic sediment transport model (7.14 hr for one calibration and 2.0 hr

for one validation run) and the therefore very limited expansion order of the aPC (second), we employ iterative Bayesian updating of the surrogate model. Through the iterations, we identify the most probable region in the space of three calibration parameters ($\theta_{\text{crit}}, k'_{St,j}\, d_i$) and refine the surrogate accordingly. The combination of strict Bayesian principles with model reduction assures that the constructed surrogate model, based on only 20 runs of the original sediment transport model, still captures effectively the morphodynamic behavior and the sediment transport processes in the Lower River Salzach. One model call of the final aPC surrogate model requires only $2 \times 6.76\,\text{ms} = 13.52$ ms for both calibration and validation. Hence, we could afford a brute-force Monte Carlo simulation (100,000 realizations) treatment of the surrogate to quantify parametric and predictive uncertainty.

In the morphodynamic sediment transport model, the initial riverbed geometry is from the year 2002. For calibration, available riverbed measurements from the years 2005 and 2010 have been used. The findings have been validated using riverbed measurements from the year 2013. Bayesian calibration and validation of the aPC surrogate model with Monte Carlo simulation provides detailed statistical information about the predicted riverbed behavior along the Lower River Salzach. The presented results show that automated Bayesian calibration helps to significantly improve the fit to data and to reduce the remaining uncertainty along the entire river. The standard deviation reduces on spatial average from 0.73 to 0.15 m during the calibration period and from 0.67 to 0.15 m during the validation period. The largest reductions in uncertainty occurred at critical spots such as the upstream region where the River Saalach mouths into the River Salzach and the region close to the downstream boundary condition.

We verified the surrogate model against the physical deterministic sediment transport model. For this, we used the best deterministic scenario corresponding to the maximum a posteriori (MAP) response of the aPC surrogate. The test indicates very good agreement between the surrogate and the full *Hydro_FT−2D* sediment transport model for both calibration ($\epsilon_{\text{Cal}} = 0.31$ m) and validation ($\epsilon_{\text{Val}} = 0.42$ m) especially when considering the spatial domain of the investigated river section of interest (6.9 km long, on average 82 m movable riverbed width). The verification results reveal that the aPC surrogate can be used to study the morphodynamic sediment transport processes in the Lower River Salzach.

In a final step, we conducted a residual analysis between the riverbed measurements and simulation results to asses the overall quality of the models for the calibration and validation period. We calculated the residuals for the stochastically calibrated surrogate model and the morphodynamic model using the MAP parameter set as well as for the manually calibrated morphodynamic model. We conclude that the surrogate-based Bayesian approach is at least as good as a manual calibration conducted in an earlier study, but requires only a fraction of the computational time (more than 8 times faster) for obtaining the results.

Overall, it can be concluded that Bayesian calibration for physical-deterministic sediment transport models, such as *Hydro_FT−2D*, by means of an aPC surrogate model, offers a significant contribution to morphodynamic river modeling. The key conclusion is that, within a significantly reduced computational time, we quantified the uncertainties, increased the robustness, and finally improved the overall quality of the calibration and validation of a large-scale and time-demanding physical-deterministic sediment transport model. This confirms the belief of Schmelter et al. (2011), that Bayesian modeling provides a tool for innovation in sediment transport research, especially when being combined with surrogate techniques to address computational time constraints (see also Mohammadi et al., 2018). The applied framework in this study is universally applicable and not confined to any physical-deterministic sediment transport model. Although aPC is a well selected specific choice (see also Köppel et al., 2019), there are more surrogate techniques, many of which will serve the same goal: speeding up the model, such that uncertainty quantification and Bayesian updating of large-scale applications becomes feasible.

Data Availability Statement

Input data to the morphodynamic sediment transport model were previously published in Beckers et al. (2016, 2018). The methods for model reduction and Bayesian updating were published in the references (Oladyshkin & Nowak, 2012, 2018; Oladyshkin, Class, et al., 2013). The codes to achieve the model reduction using Data-driven Arbitrary Polynomial Chaos (aPC) are available at this site (https://mathworks.com/matlabcentral/fileexchange/72014-apc-matlab-toolbox-data-driven-arbitrary-polynomial-chaos). The codes

that combine aPC with strict Bayesian principles for stochastic model calibration and parameter inference are available at this site (https://mathworks.com/matlabcentral/fileexchange/74006-bapc-matlab-toolbox-bayesian-arbitrary-polynomial-chaos). The model outputs as well as the calibration and validation data are accessible at Zenodo (Beckers et al., 2019).

Acknowledgments
The authors would like to thank the German Research Foundation (DFG) for their financial support of the project through the Cluster of Excellence "Data-Integrated Simulation Science" (EXC 2075) at the University of Stuttgart. The data used in this study were provided by the water authority Traunstein (WWA Traunstein) and the state government of Salzburg (ASL Salzburg).

References

Ackers, P., & White, W. R. (1973). Sediment transport: New approach and analysis. *Journal of the Hydraulics Division*, *99*(11), 2041–2060.
Aquaveo (2013). SMS user manual (v11.1) Surface-water modeling System.
Beckers, F., Heredia, A., Noack, M., Nowak, W., Wieprecht, S., & Oladyshkin, S. (2019). Data related to the manuscript "Bayesian calibration and validation of a large-scale and time-demanding sediment transport model". Zenodo, Data set (Version 1), https://doi.org/10.5281/zenodo.3576395
Beckers, F., Noack, M., & Wieprecht, S. (2016). Geschiebetransportmodellierung (GTM) Salzach und Saalach [Bed load transport modeling of the rivers Salzach and Saalach] (*08a/2015 and 08b/2015*). Stuttgart: Institute for Modelling Hydraulic and Environmental Systems (IWS) Department of Hydraulic Engineering and Water Resources Management.
Beckers, F., Noack, M., & Wieprecht, S. (2018). Uncertainty analysis of a 2D sediment transport model: An example of the lower river Salzach. *Journal of Soils and Sediments*, *18*, 3133–3144.
Box, G. E. P., & Tiao, G. C. (1973). Bayesian inference in statistical analysis. Addison-Wesley Publishing Company.
Buffington, J. M., & Montgomery, D. R. (1997). A systematic analysis of eight decades of incipient motion studies, with special reference to gravel-bedded rivers. *Water Resources Research*, *33*, 1993–2029.
Chavarrías, V., Stecca, G., & Blom, A. (2018). Ill-posedness in modeling mixed sediment river morphodynamics. *Advances in Water Resources*, *114*, 219–235.
Cunge, J. A., Holly, F. M., & Verwey, A. (1980). *Practical aspects of computational river hydraulics*, *Monographs and surveys in water resources engineering*. Boston: Pitman Advanced Pub. Program.
Engelund, F., & Hansen, E. (1967). *A monograph on sediment transport in alluvial streams*. Copenhagen: Teknisk Forlag.
Exner, F. M. (1925). Ueber die Wechselwirkung zwischen Wasser und Geschiebe in Flssen [On the interaction between water and bed load in rivers]. *Sitzungsberichte d. Akad. d. Wiss., math.-naturw. Klasse, Abt II a*, 43 de.
Habersack, H., & Pigay, H. (2007). 27 River restoration in the Alps and their surroundings: Past experience and future challenges, *Developments in Earth Surface Processes* (vol. 11, pp. 703–735): Elsevier en.
Hinderer, M., Kastowski, M., Kamelger, A., Bartolini, C., & Schlunegger, F. (2013). River loads and modern denudation of the Alps—A review. *Earth-Science Reviews*, *118*, 11–44.
Hirano, M. (1971). River-bed degradation with armoring. *Proceedings of the Japan Society of Civil Engineers*, *1971*(195), 55–65.
Hunziker, R. P. (1995). Fraktionsweiser Geschiebetransport [Multi-fraction bed load transport], *Communications of the Laboratory of Hydraulics, Hydrology and Glaciology of the ETH Zürich*. Zürich, Switzerland.
Hunziker, R. P., & Jaeggi, M. N. R. (2002). Grain sorting processes. *Journal of Hydraulic Engineering*, *128*(12), 1060–1068.
James, S. C., Jones, C., Grace, M., & Roberts, J. (2010). Recent advances in sediment transport modeling. *Journal of Hydraulic Research*, *48*(6), 754–763.
Kass, R. E., & Raftery, A. E. (1995). Bayes factors. *Journal of the American Statistical Association*, *90*(430), 773–795.
Kim, Y. J., & Park, C. S. (2016). Stepwise deterministic and stochastic calibration of an energy simulation model for an existing building. *Energy and Buildings*, *133*, 455–468.
Klar, R., Achleitner, S., Jocham, S., & Aufleger, M. (2014). Calibration strategies designed for long term sediment transport modelling. CUNY Academic Works.
Klar, R., Achleitner, S., Umach, L., & Aufleger, M. (2012). Long-term simulation of 2D fractional bed load transport benefits and limitations of a distributed computing approach. In *HIC 2012: Understanding changing climate and environment and finding solutions*, 10th International Conference on Hydroinformatics, Hamburg, Germany, pp. 9.
Kondolf, G. M., & Pinto, P. J. (2017). The social connectivity of urban rivers. *Geomorphology*, *277*, 182–196.
Kostof, S., & Castillo, G. (2005). *The city assembled: the elements of urban form through history*. New York, NY: Thames & Hudson.
Köppel, M., Franzelin, F., Krker, I., Oladyshkin, S., Santin, G., Wittwar, D., et al. (2019). Comparison of data-driven uncertainty quantification methods for a carbon dioxide storage benchmark scenario. *Computational Geosciences*, *23*(2), 339–354.
Loeven, G. J. A., Witteveen, J. A. S., & Bijl, H. (2007). Probabilistic collocation: An efficient non-intrusive approach for arbitrarily distributed parametric uncertainties. In *45th AIAA Aerospace Sciences Meeting and Exhibit*, American Institute of Aeronautics and Astronautics, Reno, Nevada.
Mangelsdorf, J., Wei, F.-H., & Schaipp, B. (2000). *Wasserwirtschaftliche Rahmenuntersuchung Salzach - Untersuchungen zur FluÃ§morphologie der Unteren Salzach [Water management framework study Salzach - Investigation of the river morphology of the Lower River Salzach]* (Report No 2). Munich: Bayerisches Landesamt fur Wasserwirtschaft.
Maren, B. V., & Wegen, M. V. D. (2016). Uncertainty in modeling fine sediment transport and morphodynamics. *Abstract for the 18th Physics of Estuaries and Coastal Seas Conference, 2016*, *1*, 1–2.
Merritt, W. S., Letcher, R. A., & Jakeman, A. J. (2003). A review of erosion and sediment transport models. *Environmental Modelling & Software*, *18*(8-9), 761–799.
Meyer-Peter, E., & Mueller, R. (1948). Formulas for bed-load transport, *Proceedings of the 2nd Meeting of the International Association for Hydraulic Structures Research* (pp. 39–64). Stockholm: IAHR English.
Mohammadi, F., Kopmann, R., Guthke, A., Oladyshkin, S., & Nowak, W. (2018). Bayesian selection of hydro-morphodynamic models under computational time constraints. *Advances in Water Resources*, *117*, 53–64.
Moritz, H. (1978). Least-squares collocation. *Reviews of Geophysics*, *16*, 421.
Muehleisen, R. T., & Bergerson, J. (2016). Bayesian calibration—What, why and how. *International High Performance Buildings Conference.*, *Paper 167*, 8 en.
Nujic, M., & Hydrotec (2017). HYDRO_AS-2D reference manual—2D-flow model for water management applications. Version 4.3.4, Aachen.
Nujic, M., Hydrotec, & Hunziker, Z. P. (2019). HYDRO_FT-2D reference guide—Add-ons to HYDRO_AS-2D for simulating sediment transport. Version 5.1.6, Aachen.

Oladyshkin, S., Class, H., Helmig, R., & Nowak, W. (2011). An integrative approach to robust design and probabilistic risk assessment for CO_2 storage in geological formations. *Computational Geosciences*, *15*(3), 565–577.
Oladyshkin, S., Class, H., & Nowak, W. (2013). Bayesian updating via bootstrap filtering combined with data-driven polynomial chaos expansions: Methodology and application to history matching for carbon dioxide storage in geological formations. *Computational Geosciences*, *17*(4), 671–687.
Oladyshkin, S., & Nowak, W. (2012). Data-driven uncertainty quantification using the arbitrary polynomial chaos expansion. *Reliability Engineering and System Safety*, *106*, 179–190.
Oladyshkin, S., & Nowak, W. (2018). Incomplete statistical information limits the utility of high-order polynomial chaos expansions. *Reliability Engineering & System Safety*, *169*, 137–148.
Oladyshkin, S., Schröder, P., Class, H., & Nowak, W. (2013). Chaos expansion based bootstrap filter to calibrate CO_2 injection models. *Energy Procedia*, *40*, 398–407.
Oreskes, N., Shrader-frechette, K., & Belitz, K. (1994). Verification, validation, and confirmation of numerical models in the Earth sciences. *Science*, *263*(5147), 641–646.
Pinto, L., Fortunato, A. B., Zhang, Y., Oliveira, A., & Sancho, F. E. P. (2012). Development and validation of a three-dimensional morphodynamic modelling system for non-cohesive sediments. *Ocean Modelling*, *57-58*, 1–14.
Recking, A. (2009). Theoretical development on the effects of changing flow hydraulics on incipient bed load motion. *Water Resources Research*, *45*, W04401. https://doi.org/10.1029/2008WR006826
Reisenbüchler, M., Bui, M. D., Skublics, D., & Rutschmann, P. (2019). An integrated approach for investigating the correlation between floods and river morphology: A case study of the Saalach River, Germany. *Science of The Total Environment*, *647*, 814–826.
Sadid, N., Beckers, F., Haun, S., Noack, M., & Wieprecht, S. (2016). An evolution volume balance approach to determine relevant discharge threshold for bed load transport. In *Hydrodynamic and Mass Transport at Freshwater Aquatic Interfaces*, GeoPlanet: Earth and Planetary Sciences, Zelechw, Poland.
Schmelter, M. L., Erwin, S. O., & Wilcock, P. R. (2012). Accounting for uncertainty in cumulative sediment transport using Bayesian statistics. *Geomorphology*, *175-176*, 1–13.
Schmelter, M. L., Hooten, M. B., & Stevens, D. K. (2011). Bayesian sediment transport model for unisize bed load. *Water Resources Research*, *47*, W11514. https://doi.org/10.1029/2011WR010754
Schmelter, M. L., & Stevens, D. K. (2013). Traditional and Bayesian statistical models in fluvial sediment transport. *Journal of Hydraulic Engineering*, *139*(3), 336–340.
Shojaeezadeh, S. A., Nikoo, M. R., McNamara, J. P., AghaKouchak, A., & Sadegh, M. (2018). Stochastic modeling of suspended sediment load in alluvial rivers. *Advances in Water Resources*, *119*, 188–196.
Simons, R. K., Canali, G. E., Anderson-Newton, G. T., & Cotton, G. K. (2000). Sediment transport modeling: Calibration, verification, and evaluation. *Soil and Sediment Contamination*, *9*(3), 261–289.
Siviglia, A., Stecca, G., Vanzo, D., Zolezzi, G., Toro, E. F., & Tubino, M. (2013). Numerical modelling of two-dimensional morphodynamics with applications to river bars and bifurcations. *Advances in Water Resources*, *52*, 243–260.
Smith, A. F. M., & Gelfand, A. E. (1992). Bayesian statistics without tears: A sampling resampling perspective. *The American Statistician*, *46*(2), 84–88.
Stecca, G., Zolezzi, G., Hicks, D. M., & Surian, N. (2019). Reduced braiding of rivers in human-modified landscapes: Converging trajectories and diversity of causes. *Earth-Science Reviews*, *188*, 291–311.
Stephan, U., Hengl, M., Hartmann, S., Otto, A., & Hunziker, R. (2002). *Wasserwirtschaftliche Rahmenuntersuchung Salzach—Geschiebetransportmodellierung [Water management framework study Salzach—Bed load transport modeling]* (Report No 4). Munich: Bayerisches Landesamt fur Wasserwirtschaft.
Stephan, U., Hengl, M., & Schaipp, B. (2003). River restoration considering geomorphological boundary conditions. In *Proceeding of the 30th IAHR Congress*, *Theme C, Inland Waters: Research, Engineering and Management*, *II*, Thessaloniki, pp. 457–464.
Strickler, A. (1923). *Beitrge zur Frage der Geschwindigkeitsformel und der Rauhigkeitszahlen fur Strme, Kanle und geschlossene Leitungen [Contributions to the questions of velocity formulations and roughness values for rivers, canals, and closed ducts]* (vol. 16). Bern, Switzerland: Eidgenssisches Amt fur Wasserwirtschaft.
Villadsen, J., & Michelsen, M. L. (1978). *Solution of differential equation models by polynomial approximation*, *Prentice-Hall international series in the physical and chemical engineering sciences*. Englewood Cliffs, NJ: Prentice-Hall.
Villaret, C., Kopmann, R., Wyncoll, D., Riehme, J., Merkel, U., & Naumann, U. (2016). First-order uncertainty analysis using algorithmic differentiation of morphodynamic models. *Computers & Geosciences*, *90*, 144–151.
Wöhling, T., Schöniger, A., Gayler, S., & Nowak, W. (2015). Bayesian model averaging to explore the worth of data for soil-plant model selection and prediction. *Water Resources Research*, *51*, 2825–2846. https://doi.org/10.1002/2014WR016292
Webster, M. D., Tatang, M. A., & McRae, G. J. (1996). Application of the probabilistic collocation method for an uncertainty analysis of a simple ocean model. MIT Joint Program on the Science and Policy of Global Change Report, 4.
Wiener, N. (1938). The homogeneous chaos. *American Journal of Mathematics*, *60*(4), 897–936.
Williams, R. D., Measures, R., Hicks, D. M., & Brasington, J. (2016). Assessment of a numerical model to reproduce event-scale erosion and deposition distributions in a braided river. *Water Resources Research*, *52*, 6621–6642. https://doi.org/10.1002/2015WR018491
Wu, F.-C., & Chen, C. C. (2009). Bayesian updating of parameters for a sediment entrainment model via Markov chain Monte Carlo. *Journal of Hydraulic Engineering*, *135*(1), 22–37.
Xiu, D., & Karniadakis, G. E. (2002). The Wiener-Askey polynomial chaos for stochastic differential equations. *SIAM Journal on Scientific Computing*, *24*(2), 619–644.